Pergamon

Int. J. Heat Mass Transfer. Vol. 39, No. 3, pp. 479–490, 1996

0017-9310/96 $9.50+0.00

0017-9130(95)00153-0

Enhancement of natural convection heat transfer from an array of discrete heat sources

T. J. HEINDEL†, F. P. INCROPERA and S. RAMADHYANI

Heat Transfer Laboratory, School of Mechanical Engineering, Purdue University, West Lafayette, IN 47907-1288, U.S.A.

(*Received* 8 *December* 1994 *and in final form* 6 *April* 1995)

Abstract—Single-phase, natural convection heat transfer data have been obtained for an array of highly-finned, discrete heat sources mounted to one wall of a cavity filled with a dielectric liquid (FC-77). Dense, parallel plate fin arrays were considered for both vertical and horizontal cavity orientations, and the finned surfaces were found to enhance heat transfer by as much as a factor of 24. Thermal resistances approaching 2 cm^2 °C W^{-1} were realized, while maintaining the temperature difference between the fin base and an opposing cold plate below 70°C. In a parallel numerical study, flow and heat transfer conditions were calculated by treating the fin array as a porous medium characterized by the Brinkman–Forchheimer–extended Darcy model. The model provided a reasonable approximation which captured the experimental trends and predicted the data to within 30%.

INTRODUCTION

Continued miniaturization of integrated circuits on a single computer chip and reduced spacing between chips in an array have contributed to significant improvements in the performance of computer systems. However, increased circuit densities increase power dissipation and complicate thermal control when a principal objective is to maintain components at or below specified maximum service temperatures [1]. Currently, thermal control is typically maintained by direct air cooling or by indirect liquid cooling [1–3]. Due to inherent heat transfer limitations, air cooling may be precluded for future workstations and desktop computers, while indirect liquid cooling would require a distribution system consisting of a pump and associated plumbing fixtures. Moreover, undesirable noise and vibration may accompany fan or pump assemblies.

In contrast, natural convection affords a means of thermal control which eliminates the fan or pump and provides a noise- and vibration-free environment. However, natural convection is not an effective mode of heat transfer, and compared to forced convection or boiling, associated thermal resistances are large. To accommodate low to moderate power dissipation levels, the computer chips would have to be directly immersed in a liquid coolant, and even then, maximum surface heat fluxes corresponding to typical chip upper temperature limits of 85°C would be of the order of 1 W cm^{-2} [4]. To surpass these limits in a passive cooling system and approach those associated with forced convection, heat transfer enhancement is necessary.

Parallel plate fin arrays are often used to enhance heat transfer by free convection. Fluid flow between the fins is usually assumed two-dimensional and can be classified into three regions [5]. In the *isolated-plate limit* ($b/H_{fin} \to \infty$), heat transfer rates approach those associated with flow along a single plate in an infinite fluid. For the *fully-developed limit* ($b/H_{fin} \to 0$), thermal boundary layers merge near the entrance, yielding fully-developed conditions in the channel formed by adjoining plates. In the *developing regime*, the fin height and spacing prevent either extreme from being realized. If the plates are close enough to allow interaction of the adjoining boundary layers, heat transfer rates diminish with decreasing b and may be correlated by the following expression developed by Elenbaas [6]:

$$\overline{Nu}_b = \frac{1}{24} Ra_b \left(\frac{b}{L_z}\right) \left\{ 1 - \exp\left[\frac{-35}{Ra_b \left(\frac{b}{L_z}\right)} \right] \right\}^{3/4} \quad (1)$$

where the average Nusselt number and Rayleigh number are based on the plate spacing b. Equation (1) assumes that the ratio of plate width-to-spacing (L_{fin}/b) is large, edge effects are negligible, and the plates are isothermal and symmetrically heated. Early experimental studies to determine the optimum geometry for parallel plate fin arrays [7–9] showed

†Current address: Institute of Paper Science and Technology, 500 10th Street NW, Atlanta, GA 30318-5794, U.S.A.

NOMENCLATURE

A_c	cross-sectional area
A_h	heater base area, L_xL_z
A_{fin}	total fin surface area
A_x	cavity aspect ratio, D/S
A_z	cavity aspect ratio, H/S
b	parallel plate fin spacing
C_F	dimensionless form drag constant in Forchheimer's extension
c_{pf}	fluid specific heat
D	cavity dimension along the x-axis
Da_b	Darcy number, K/b^2
g	gravitational acceleration
H	cavity dimension along the z-axis
H_{fin}	fin height parallel to the fin base
$\bar{h}$	average convection heat transfer coefficient
K	permeability
k	thermal conductivity
L_{fin}	fin length from the fin base to the fin tip
L_x	length of heater base in the x-direction
L_z	length of heater base in the z-direction
m	fin parameter, $\sqrt{[\bar{h}P/(k_{fin}A_c)]}$
$\overline{Nu}_b$	average Nusselt number based on fin plate spacing
N_{fin}	total number of parallel plate fins per heater or cold plate
P	perimeter
P_{fin}	parallel plate fin pitch
Pr	Prandtl number, v/α_f
p	pressure
Q	power dissipation rate per heater
q''	heat flux based on heater base area, Q/A_h
Ra_b	Rayleigh number based on fin plate spacing, $g\beta(T_{sur}-T_r)b^3Pr/v^2$
Ra_{L_z}	Rayleigh number based on heater length, $g\beta(T_{sur}-T_c)L_z^3Pr/v^2$
$Ra^*_{L_z}$	modified Rayleigh number, $g\beta q''L_z^4/(k_f\alpha_f v)$
R''_{th}	thermal resistance, $(\bar{T}_{sur,(i,j)}-T_c)/q''$
S	cavity dimension along the y-axis
T	temperature
T_c	cold plate temperature
T_r	reference temperature
V, W	dimensionless velocities, vL_z/α_f and wL_z/α_f
v, w	velocity components
y, z	coordinate directions.

Greek symbols

α_f	fluid thermal diffusivity
β	volumetric thermal expansion coefficient
δ_{fin}	parallel plate fin thickness
ζ	binary parameter
η_{fin}	fin efficiency
θ	dimensionless temperature, $(T-T_c)/(q''L_z/k_f)$
ε_{fin}	fin effectiveness
μ	dynamic viscosity
v	kinematic viscosity
ρ	fluid density
ϕ	cavity orientation
φ	porosity
Ψ	dimensionless streamfunction.

Subscripts

eff	effective
f	fluid
fin	fin
(i,j)	heater (i,j)
max	maximum
Ri	row i
sur	surface
t	total.

Superscript

$\bar{}$	average.

that the Elenbaas correlation [6] can be applied to parallel plate fins when $Ra_b(b/H_{fin}) \gtrsim 100$.

Using the Elenbaas correlation, Bar-Cohen [10] analyzed an array of longitudinal fins to determine optimal spacing and thickness corresponding to the maximum heat dissipation. Bar-Cohen and Rohsenow [11] extended this analysis to include other boundary conditions, such as adjacent isoflux plates. Additionally, Bar-Cohen and Jelinek [12] determined that the fin spacing should equal the fin thickness for an optimum least material fin. Other investigators who have performed optimization studies for natural convection between vertical parallel plates include Hung and Lu [5], Aihara and Maruyama [13], and, most recently, Anand *et al.* [14].

Densely packed, parallel plate fins may be thought of as a porous medium. Simulations of natural convection in enclosures partially filled with porous media have been completed [15, 16]. Recent theoretical treatments in which spirally fluted tubes have been modeled as a porous medium include studies by Srinivasan *et al.* [17].

The purpose of this study is to present experimental data and numerical predictions of heat transfer from a 3×3 array of discrete heat sources mounted to one wall of a cavity with an isothermally cooled opposing

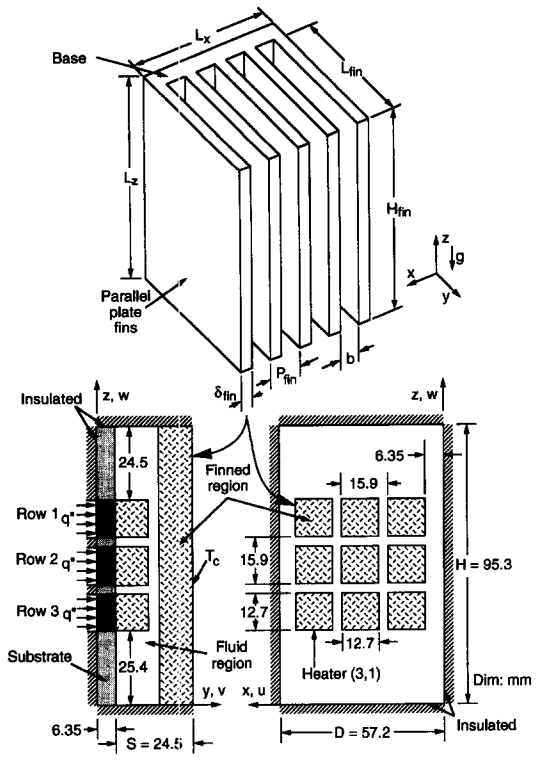

Fig. 1. Fin array and test cell geometry.

wall (Fig. 1). The surface of each discrete heat source and the cold wall were augmented by dense arrays of parallel plate fins. A dielectric liquid coolant (FC-77, a dielectric liquid manufactured by 3M Co.) was used as the heat transfer medium and thermal resistances were determined for $(\bar{T}_{sur,(i,j)} - T_c) \lesssim 70°C$. Numerical predictions, based on the Brinkman–Forchheimer–extended Darcy model for porous media, were also obtained and compared to the experimental results.

EXPERIMENTAL PROCEDURES

The parallel plate fin arrays used in this study (Fig. 1) were designed for maximum power dissipation (details are provided in Appendix A). The dimensions of the enhanced surface are L_x and L_z, respectively, forming a base area of $A_h = L_x L_z$. The fin length, L_{fin}, is the distance from the base of the fin to the fin tip, while the fin height, H_{fin}, determines the extent of the fin along the base. The fin thickness, spacing, and pitch are designated by δ_{fin}, b and P_{fin}, respectively.

The test cell, shown schematically in Fig. 2 with dimensions provided in Fig. 1, consisted of a 3×3 array of highly-finned copper elements mounted in a G-10 substrate, an opposing highly-finned copper cold plate, and a Lexan spacer. The cell was compressed between two aluminum clamping plates, and O-rings were used to seal the interfaces between components. Two threaded holes were located near the top of the substrate to allow for filling and draining of the test cell, and polyethylene tubing, with the free end open to the atmosphere, was attached to each hole to allow for fluid expansion.

Approximately 0.2 mm of material was carefully milled from the back of each fin array to provide a smooth, even surface for attachment of a resistive element. Two holes were drilled from the back to a distance of 2 mm from the fin base, and copper-constantan thermocouples were inserted into each hole and soft-soldered into place. A thick-film resistive element, powered by a d.c. source, was soldered to the back of the finned surface, forming the discrete heat source. The finned heater array was then assembled and fixed in place with epoxy, such that the fin base was flush with the substrate surface and the fin arrays were aligned from column-to-column.

The finned cold plate attachment was soldered into a pocket formed on a copper plate which contained an internal maze of channels through which water from a constant temperature bath could be circulated. Copper–constantan thermocouples were then inserted into three holes drilled from the back surface to a distance of 3.2 mm from the fin base.

A spacer plate thickness of $S = 24.5$ mm provided cavity aspect ratios of $A_z = H/S = 3.75$ and $A_x = D/S = 2.25$, and a clearance of 1.4 mm between the heater and cold plate fin tips. Experiments were conducted with degassed FC-77. All heaters were equally powered, and steady-state temperatures and power inputs were recorded by an HP data acquisition system interfaced to a personal computer.

All tests were conducted under conditions of equal power dissipation (Q). A three-dimensional (3D) finite-difference conduction analysis of the heater substrate revealed that more than 98% of the energy applied to the resistive element entered the fluid through the heater base [18]. Assuming a uniform heat flux through each fin base, the heater and cold plate surface temperatures were inferred by assuming 1D heat conduction between the thermocouple locations and the fin base. The cold plate temperature was maintained at approximately 15°C for all tests.

The overall thermal resistance of each heater, R''_{th}, was used to assess the thermal performance of the finned heat sources, with

$$R''_{th} = \frac{A_h(\bar{T}_{sur,(i,j)} - T_c)}{Q_{(i,j)}} \quad (2)$$

where $\bar{T}_{sur,(i,j)}$ and T_c are the average surface temperatures of heater (i,j) and the cold plate, respectively, and $Q_{(i,j)}$ is the measured applied power at the resistive element. Heater (i,j) refers to the heater in row i and column j (heater (3,1) is specified in Fig. 1). The base area, A_h, of the heater was used to facilitate comparisons with data for unfinned heaters in a similar geometric arrangement [18]. Maximum uncertainties in the reported thermal resistances and temperature differences, as estimated by the procedure of Kline and McClintock [19], were 9.4 and 5.0%, respectively.

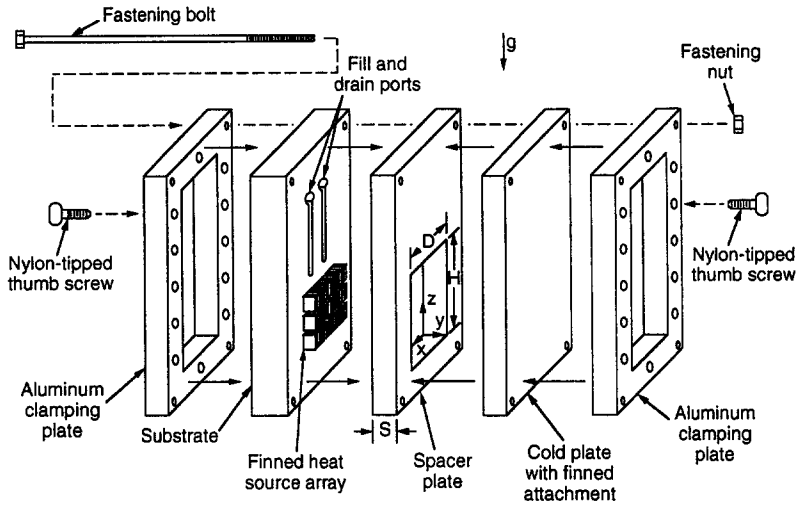

Fig. 2. Test cell schematic.

NUMERICAL MODEL

Porous medium model

The dense parallel plate fin array was approximated as a porous medium, which allowed a 2D approximation of the fin array. Hence, the actual 3×3 array of discrete heat sources was represented as a 3×1 array of strip heaters, and 2D calculations replaced full 3D simulations, thereby greatly reducing the required computational effort. Since non-Darcian effects can be significant [15, 20], a Brinkman–Forchheimer–extended Darcy model was used in this study. The model uses physically realistic boundary conditions at the fluid–porous medium interfaces (Brinkman's extension) and accounts for inertia effects (Forchheimer's extension). Both boundary and inertia effects decrease heat transfer with increasing Rayleigh number [21]. The porous medium is considered to be homogeneous and isotropic and to be saturated with fluid which is in local thermodynamic equilibrium with the solid matrix.

Throughout the cavity, flow is assumed to be laminar, 2D, incompressible, and steady, and in accordance with to the Boussinesq approximation, all properties are assumed constant. In unfinned regions of the cavity, conditions are characterized by the following form of the Navier–Stokes equations:

Continuity:

$$\frac{\partial v}{\partial y} + \frac{\partial w}{\partial z} = 0 \tag{3}$$

y-Momentum:

$$\rho\left[v\frac{\partial v}{\partial y} + w\frac{\partial v}{\partial z}\right] = -\frac{\partial p}{\partial y} + \mu_f\left[\frac{\partial^2 v}{\partial y^2} + \frac{\partial^2 v}{\partial z^2}\right] \tag{4}$$

z-Momentum:

$$\rho\left[v\frac{\partial w}{\partial y} + w\frac{\partial w}{\partial z}\right] = -\frac{\partial p}{\partial z} + \mu_f\left[\frac{\partial^2 w}{\partial y^2} + \frac{\partial^2 w}{\partial z^2}\right] + \rho g\beta(T - T_c) \tag{5}$$

Energy:

$$\rho\left[v\frac{\partial T}{\partial y} + w\frac{\partial T}{\partial z}\right] = \frac{k_f}{c_{pf}}\left[\frac{\partial^2 T}{\partial y^2} + \frac{\partial^2 T}{\partial z^2}\right]. \tag{6}$$

In contrast, using the Brinkman–Forchheimer–extended Darcy model with a superficial (Darcian) velocity, governing equations for the finned regions of the cavity are of the following form:

Continuity:

$$\frac{\partial v}{\partial y} + \frac{\partial w}{\partial z} = 0 \tag{7}$$

y-Momentum:

$$0 = -\frac{\partial p}{\partial y} + \mu_{eff}\left[\frac{\partial^2 v}{\partial y^2} + \frac{\partial^2 v}{\partial z^2}\right] - \left[\frac{\rho C_F}{\sqrt{K}}|\mathbf{V}| + \frac{\mu_f}{K}\right]v \tag{8}$$

z-Momentum:

$$0 = -\frac{\partial p}{\partial z} + \mu_{eff}\left[\frac{\partial^2 w}{\partial y^2} + \frac{\partial^2 w}{\partial z^2}\right] - \left[\frac{\rho C_F}{\sqrt{K}}|\mathbf{V}| + \frac{\mu_f}{K}\right]w + \rho g\beta(T - T_c) \tag{9}$$

Energy:

$$\rho\left[v\frac{\partial T}{\partial y} + w\frac{\partial T}{\partial z}\right] = \frac{k_{eff}}{c_{pf}}\left[\frac{\partial^2 T}{\partial y^2} + \frac{\partial^2 T}{\partial z^2}\right] \tag{10}$$

where

$$|\mathbf{V}| = \sqrt{(v^2 + w^2)} \tag{11}$$

and the permeability K of the porous matrix can be determined by modeling the parallel plate fins as a

stack of capillary fissures of width b and fissure thickness δ_{fin}. For this geometry, Bear [22] suggests the relation

$$K = \frac{\varphi b^2}{12} = \frac{b^3}{12(\delta_{fin}+b)} \tag{12}$$

where the porosity φ is defined as the ratio of void volume to total volume of the porous structure.

While standard advection terms in the momentum equations are generally small for a porous medium and are typically neglected [23, 24], Nield and Bejan [25] recommend that the corresponding nonlinear inertia effects be treated by the Forchheimer drag term, which includes a dimensionless form drag coefficient, C_F. This coefficient depends on the nature of the porous medium and, as a first approximation, can be determined from the following empirical formula [26]

$$C_F = K^{1/2} 1.75 \frac{(1-\varphi)}{\varphi^3 b} \tag{13}$$

where the fin spacing b is used as the characteristic length of the porous material. Although the Brinkman extension necessitates determination of an effective dynamic viscosity, μ_{eff}, of the volume-averaged porous medium, accurate predictions may be obtained with the approximation $\mu_{eff} = \mu_f$ [16, 27, 28].

Advection terms must be retained in the energy equation [23] and a realistic model must be prescribed for the effective thermal conductivity, k_{eff}. While many different models have been developed to predict the effective thermal conductivity [29, 30], the following expression was used for the parallel plate fin configuration of this study

$$k_{eff} = (1-\varphi)k_{fin} + \varphi k_f. \tag{14}$$

It represents a weighted arithmetic mean based on the presumption of parallel conduction paths through the fluid and fins. Although the thermal conductivity is anisotropic in the actual fin array, with a parallel conduction path in the fin direction and a series conduction path perpendicular to the fins, the parallel conduction path is dominant and equation (14) provides a reasonable approximation.

Introducing the following binary parameter

$$\zeta(y,z) = \begin{cases} 1 \text{ in the porous region} \\ 0 \text{ in the fluid region} \end{cases} \tag{15}$$

the separate equations for the fluid and porous regions may be combined into a single set. In terms of a superficial (Darcian) velocity, the resulting equations are of the following form:

Continuity:

$$\frac{\partial v}{\partial y} + \frac{\partial w}{\partial z} = 0 \tag{16}$$

y-Momentum:

$$(1-\zeta)\rho\left[v\frac{\partial v}{\partial y} + w\frac{\partial v}{\partial z}\right] = -\frac{\partial p}{\partial y} + \mu_f\left[\frac{\partial^2 v}{\partial y^2} + \frac{\partial^2 v}{\partial z^2}\right] - \zeta\left[\frac{\rho C_F}{\sqrt{K}}|\mathbf{V}| + \frac{\mu_f}{K}\right]v \tag{17}$$

z-Momentum:

$$(1-\zeta)\rho\left[v\frac{\partial w}{\partial y} + w\frac{\partial w}{\partial z}\right] = -\frac{\partial p}{\partial z} + \mu_f\left[\frac{\partial^2 w}{\partial y^2} + \frac{\partial^2 w}{\partial z^2}\right] - \zeta\left[\frac{\rho C_F}{\sqrt{K}}|\mathbf{V}| + \frac{\mu_f}{K}\right]w + \rho g\beta(T-T_c) \tag{18}$$

Energy:

$$\rho\left[v\frac{\partial T}{\partial y} + w\frac{\partial T}{\partial z}\right] = \left[(1-\zeta)\frac{k_f}{c_{pf}} + \zeta\frac{k_{eff}}{c_{pf}}\right]\left[\frac{\partial^2 T}{\partial y^2} + \frac{\partial^2 T}{\partial z^2}\right]. \tag{19}$$

Idealized boundary conditions are applied at the substrate–fluid, heater–porous medium and cold plate–porous medium interfaces and are summarized as follows:

$$\text{At } y = 0: \quad v = w = 0 \tag{20}$$

$$\frac{\partial T}{\partial y} = \begin{cases} 0 \text{ (at the substrate–fluid interface)} \\ \dfrac{-q''}{k_{eff}} \text{ (at the heater–porous medium interface)} \end{cases} \tag{21}$$

$$\text{At } y = S: \quad v = w = 0 \tag{22}$$

$$T = T_c \tag{23}$$

$$\text{At } z = 0 \text{ and } z = H: \quad v = w = 0 \tag{24}$$

$$\frac{\partial T}{\partial z} = 0. \tag{25}$$

Additional boundary conditions at the fluid–porous medium interface must ensure velocity, shear stress, temperature, and heat flux continuity. These matching conditions are explicitly imposed in the numerical solution by using the harmonic mean formulation for the interface conductivities and viscosities [31].

Results of the calculations are presented in terms of nondimensional quantities, with the heater length, L_z, selected as the appropriate length scale. A dimensionless streamfunction is defined by the relations

$$V = \frac{\partial \Psi}{\partial Z} \quad W = -\frac{\partial \Psi}{\partial Y} \tag{26}$$

where V and W are dimensionless velocities. The applied heat flux is used to define a modified Rayleigh number, $Ra^*_{L_z} = g\beta q'' L_z^4/k_f\alpha_f\nu$ and to determine a dimensionless temperature field, $\theta = k_f(T-T_c)/q''L_z$. Additionally, for comparison with experimental results, a thermal resistance is defined as

$$R''_{\text{th}} = \frac{\Delta \bar{T}}{q''} = \frac{\dfrac{1}{L_z}\displaystyle\int_{L_z} (T(y,z)|_{y=0} - T_c)\,\mathrm{d}z}{q''}. \quad (27)$$

Solution procedure

The governing equations were discretized using a control-volume formulation [31], where the velocity control volumes were staggered with respect to the pressure and temperature control volumes. The resulting algebraic equations were solved iteratively using a line-by-line application of the tri-diagonal matrix algorithm enhanced by an additive–correction multigrid method [18] to speed convergence. The additive–correction multigrid method used in this study is described in detail by Hutchinson and Raithby [32] and Hutchinson *et al.* [33]. Coupling of the pressure and velocity fields was treated using the SIMPLER algorithm [31]. Appropriate thermophysical properties were specified in each region, the governing equations were reduced to the appropriate forms in each region, and to enhance the convergence of the numerical algorithm, the left-hand side of the momentum equations was solved as if $\zeta = 0$. Since fluid velocities and velocity gradients in the porous region are small, the additional advection terms do not introduce significant errors in the predicted values.

A 52×80 nonuniform fine grid was used to solve the governing equations, and two additional coarse grids were used to generate grid correction factors for the additive–correction multigrid scheme [18]. In the limit of a converged solution, the grid correction factors approached zero. Care was taken in the deployment of all grid levels to ensure that all interfaces of discontinuity in the material properties were represented by grid control surfaces. For example, the porous–fluid interfaces were prescribed as control surfaces at every grid level. This procedure prevented the same correction from being applied over different material regions.

The overall solution procedure involved using a previously generated solution at a lower modified Rayleigh number as input to the calculations at a higher modified Rayleigh number. Original solutions at $Ra^*_{L_z} = 10^6$ were obtained by specifying very small values (on the order of 10^{-10}) for the initial velocity and temperature distributions. Under-relaxation techniques were used in the momentum equations, with relaxation factors set at 0.85 for $Ra^*_{L_z} = 10^6$. As the modified Rayleigh number increased, the relaxation factors were slowly decreased. It was found that a very slight under-relaxation of the energy equation aided the solution process, particularly at higher modified Rayleigh numbers.

Solutions were deemed to be converged after three criteria were satisfied. First, the maximum mass source, when compared to the maximum mass flux across a fine-grid control surface, was required to be below 10^{-3}. Second, the iteration-to-iteration change was examined at every fine-grid nodal point for all calculated values. However, to reduce the likelihood of false convergence related to small, but persistent, changes between successive iterations due to under-relaxation, the examinations were implemented between iterations i and i-20. The change in computed value, when compared to the maximum value in the domain, was required to be less than 0.5% for a converged solution to be realized. Finally, satisfaction of the overall energy balance was required to within 1%. Typically, the second criterion was the last to be satisfied.

To validate the model and solution procedure, natural convection in a square enclosure filled with a porous medium was simulated. Satisfactory agreement with the results of Beckermann *et al.* [15] and Lauriat and Prasad [20] were obtained. The experimental conditions of Beckermann *et al.* [28], with a fluid region adjacent to a porous region, were also modeled and good agreement between predictions and measurements was obtained. Details of these validation studies are presented by Heindel [18].

To ensure grid independence, grid studies were performed at the highest modified Rayleigh number where the velocity and thermal boundary layers are thinnest [18]. Increasing the grid size from 52×80 to 66×106 provided little variation in the streamlines and isotherms, and produced maximum deviations of 0.5 and 6.0% in the predicted thermal resistance and maximum velocity, respectively, indicating that the 52×80 grid provided a good compromise between computational effort and accuracy.

RESULTS

Experimental data

Experimental results for the thermal resistance are presented in Fig. 3 as a function of the average surface temperature difference for each heater when the cavity is vertically oriented ($\phi = 0°$). The results encompass

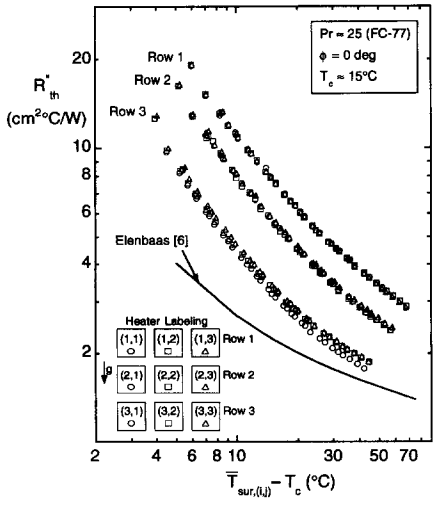

Fig. 3. Thermal resistance of the finned heater array in a vertical ($\phi = 0°$) cavity.

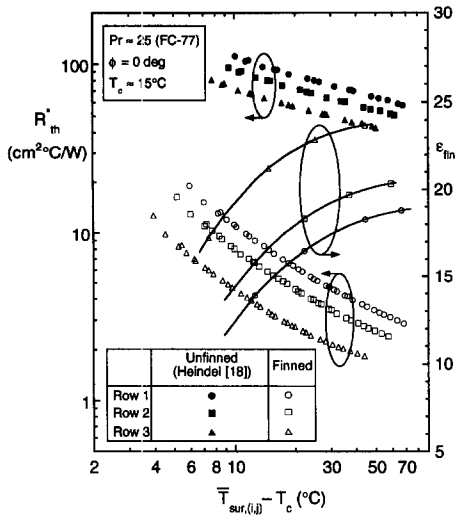

Fig. 4. Thermal resistances obtained from finned and flush-mounted arrays of discrete heat sources in a vertical ($\phi = 0°$) cavity.

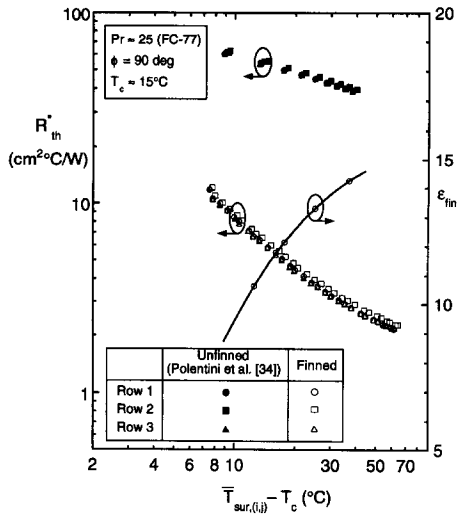

Fig. 5. Thermal resistances obtained from finned and flush-mounted arrays of discrete heat sources in a horizontal ($\phi = 90°$) cavity.

heater powers in the range $0.5 \lesssim Q \lesssim 38$ W, corresponding to $5.3 \times 10^8 \lesssim Ra^*_{L_z} \lesssim 8.0 \times 10^{10}$ ($2.0 \times 10^6 \lesssim Ra_{L_z} \lesssim 1.0 \times 10^8$). Column-to-column variations in the data are negligible for rows 1 and 2, and the small variations evident for row 3 are attributed to slight variations in the instrumentation and assembly process. Row 3 shows the lowest thermal resistance, with a minimum value of $R''_{th} = 1.84$ cm^2 °C^{-1} W^{-1} obtained for the largest temperature difference. As the fluid is heated, it ascends past rows 2 and 1, and the attendant thermal boundary layer development yields increasing values of R''_{th} with decreasing row number. Maximum surface temperatures of $\bar{T}_{sur,R1,max} = 84.0$°C, $\bar{T}_{sur,R2,max} = 73.9$°C and $\bar{T}_{sur,R3,max} = 52.8$°C were obtained for $Q \approx 38.0$ W heater^{-1}, which corresponds to a heat flux, based on fin base area, of $q'' \approx 23.6$ W cm^{-2}. These results pertain exclusively to single-phase natural convection. Predictions based on the Elenbaas [6] correlation for isothermal parallel plates, equation (1), are also shown in Fig. 3. This correlation provides reasonable agreement with the row 3 results for larger temperature differences, which is consistent with the requirement that $Ra_b\, b/H_{fin} \gtrsim 100$ for application of the correlation to plate fin arrays [7–9]. This restriction corresponds to $(\bar{T}_{sur,(i,j)} - T_c) \gtrsim 30$°C in the current study.

Row averaged thermal resistances are compared to those obtained in a similar geometry with unfinned, flush-mounted surfaces [18] in Fig. 4. Although the flush-mounted data were obtained in a cavity with aspect ratio $A_z = 7.5$, while the finned data were obtained for $A_z = 3.75$, heat transfer has been shown to be independent of aspect ratio in this range [34]. While increasing the heat transfer surface area 35-fold, the fins decrease the thermal resistance by a factor of approximately 12 for row 1 with $(\bar{T}_{sur,(i,j)} - T_c) \approx 10$°C and by as much as a factor of 24 for row 3 with $(\bar{T}_{sur,(i,j)} - T_c) \approx 45$°C. This behavior is consistent with dependence of the fin effectiveness, $\varepsilon_{fin} \equiv R''_{th}$ (unfinned)/R''_{th}(finned), on row number and temperature difference. Due to fluid heating, ε_{fin} decreases with decreasing row number. However, because higher velocities are associated with larger temperature differences, enhancing fluid penetration into the finned regions, ε_{fin} increases with increasing temperature difference. The effectiveness asymptotes to a constant value with increasing temperature difference, as fluid penetration becomes uniform throughout the fin array.

Additional data were collected over the range $1.0 \lesssim Q \lesssim 45.5$ W, corresponding to $1.1 \times 10^9 \lesssim Ra^*_{L_z} \lesssim 9.1 \times 10^{10}$ ($6.0 \times 10^6 \lesssim Ra_{L_z} \lesssim 1.0 \times 10^8$), with the cavity rotated 90° to orient the finned heat sources and cold plate on the cavity bottom and top, respectively. Since negligible column-to-column variations were observed, row-averaged thermal resistances are shown in Fig. 5. Fluid motion in the cavity was observed to be symmetric about row 2, with nearly equivalent thermal conditions for rows 1 and 3. Due to fluid preheating in these rows, fluid entering row 2 is warmer, yielding slightly higher values of R''_{th}. Overall, however, there is good uniformity in thermal conditions from row-to-row for the horizontal configuration. This behavior is consistent with the results of Polentini *et al.* [34] for flush-mounted surfaces, whose data are also included in the figure for comparison. The minimum measured row-averaged thermal resistances produced by the fins are 2.16, 2.27 and 2.19 cm^2 °C^{-1} W^{-1}, corresponding to maximum average surface temperatures of 76.4, 79.3 and 76.8°C for rows 1, 2 and 3, respectively, with $Q \approx 45.5$ W heater^{-1} and $T_c \approx 15$°C. This power dissipation rate corresponds to a heat flux of $q'' \approx 28.2$ W cm^{-2}. Results for the fin effectiveness also exhibited negligible row-to-row variations, and ε_{fin} again increased with increasing

$(\bar{T}_{\mathrm{sur},(i,j)} - T_c)$. For $(\bar{T}_{\mathrm{sur},(i,j)} - T_c) \approx 9$ and $(\bar{T}_{\mathrm{sur},(i,j)} - T_c) \approx 40$, respectively, the fins enhance heat transfer by factors of approximately 7.5 and 14.5.

Thermal resistances obtained for the horizontal orientation are within approximately 10% of those obtained for row 2 in the vertical cavity. This result suggests that a horizontal alignment of discrete heat sources is preferred when uniform heat transfer rates are desired from each row, which is most often the case for electronic cooling. Also, while maintaining acceptable temperature differences with only single-phase natural convection, thermal resistances approaching 2 $\mathrm{cm}^2\ ^\circ\mathrm{C}^{-1}\ \mathrm{W}^{-1}$ can be expected with the finned heat sources used in this study.

Numerical predictions

Numerical predictions encompassed a modified Rayleigh number range of $10^6 \leqslant Ra^*_{L_z} \leqslant 10^{11}$. The presence of the porous medium allows laminar flow conditions to be maintained at even the largest modified Rayleigh number. All calculations were performed for a 2D approximation (the y–z plane) of the geometry shown in Fig. 1, with the Prandtl number fixed at 25 (FC-77). Parameters describing the porous medium were also fixed and are summarized in Table 1. These values correspond to those representing the dense parallel plate fin arrays used in the experiments.

The effect of modified Rayleigh number on the dimensionless streamlines (Ψ) and isotherms (θ) is shown in Fig. 6. The darkened regions along the z-axis indicate the heat source locations, and the shaded regions enclosed by dashed lines represent the extent of the porous regions. At $Ra^*_{L_z} = 10^6$ [Fig. 6(a)], fluid flow is very slow ($|\Psi|_{\max} = 39.1$), as only a few streamlines penetrate the porous regions and most of the flow is confined to fluid above row 1. The flow intensity increases with increasing $Ra^*_{L_z}$, altering the streamlines considerably. Although the highest velocities and velocity gradients are still associated with fluid above row 1, porous regions adjacent to the heaters and cold plate show substantial fluid penetration, and at $Ra^*_{L_z} = 10^{11}$ [Fig. 6(b)], circulation is very intense ($|\Psi|_{\max} = 3373$) in the porous regions, as well as in the fluid. Fluid in the gaps between the porous regions is discernible by the abrupt bending of streamlines. The small gap between the hot and cold wall porous regions provides a substantially reduced resistance to flow and is hence the site of strong downflow, penetrating to the cavity floor. Fluid in the cold porous region is prevented from descending this far because of the higher drag associated with penetration of this region to the bottom of the cavity. A portion of the downflow penetrates the fluid gaps between the heated porous regions, creating small recirculation cells near the leading and trailing edges of the row 2 porous region ($y/L_z \approx 0.95$, $z/L_z \approx 3.25$ and 4.25). Fluid velocities decrease upon entering the row 3 porous region, causing very small recirculation cells to form in the fluid below this region. The intensity of these cells is very low ($\Psi = 60.9$) compared to the main flow ($\Psi = -3373$), and they are located within the zero streamlines protruding from the hot wall.

Table 1. Porous medium parameters associated with the parallel plate fin arrays used in this study

	Heater array	Cold plate array
Da_b	6.0×10^{-2}	6.0×10^{-2}
K	$1.56 \times 10^{-8}\ \mathrm{m}^2$	$1.56 \times 10^{-8}\ \mathrm{m}^2$
φ	0.718	0.718
C_F	0.327	0.327
k_{eff}	$112.8\ \mathrm{W\ m^{-1}\ K^{-1}}$	$112.8\ \mathrm{W\ m^{-1}\ K^{-1}}$

Figure 6 also displays the effect of modified Rayleigh number on the nondimensional temperature distribution, θ. Due to negligible circulation and a high effective thermal conductivity, nearly isothermal conditions exist in the porous regions for $Ra^*_{L_z} = 10^6$ [Fig. 6(c)]. Fluid adjacent to the leading edge of row 3 is thermally stratified, and large temperature gradients exist between the hot and cold wall porous regions, as shown by the merging of isotherms to form a black band in the gap between these two regions. Temperature variations in the fluid above row 1 are caused by localized convection in this region.

Even though large temperature gradients exist at the fluid–porous region interfaces for $Ra^*_{L_z} = 10^{11}$ [Fig. 6(d)], increased fluid penetration into the porous regions increases thermal variations within these regions. Large temperature variations are observed near the hot wall at $z/L_z \approx 2.0$, 3.25 and 4.5, which are locations corresponding to fluid–porous region interfaces. The porous region adjacent to the cold wall also displays thermal variations, but they are confined to upper regions, with nearly isothermal conditions prevailing in the lower region. The strong downflow in the gap between the hot and cold regions advects relatively warm fluid below row 3, causing the isotherms to bend at the leading edge of the row 3 porous region.

Nield and Bejan [25] indicate that fluid advection modeled by Forchheimer's extension is negligible if the Reynolds number, based on a typical pore diameter, is of order unity or smaller. Since the maximum channel Reynolds number is approximately 7 for the conditions of this study, the influence of Forchheimer's term should be small. Additional calculations were performed by employing the Brinkman–extended Darcy porous medium model [$C_F \equiv 0$ in equations (8) and (9)], over the range $10^6 < Ra^*_{L_z} \leqslant 10^{11}$. Neglecting Forchheimer's extension increased velocities in the porous regions and decreased the associated temperatures. However, differences between model predictions were negligible for $Ra^*_{L_z} \lesssim 10^8$. At $Ra^*_{L_z} = 10^{11}$, maximum deviations in $|\Psi|_{\max}$ and $\theta_{\max}$ were limited to approximately 25%.

Predicted thermal resistances are compared with experimental results in Fig. 7. The predictions follow the experimental trends, with the Brinkman–Forch-

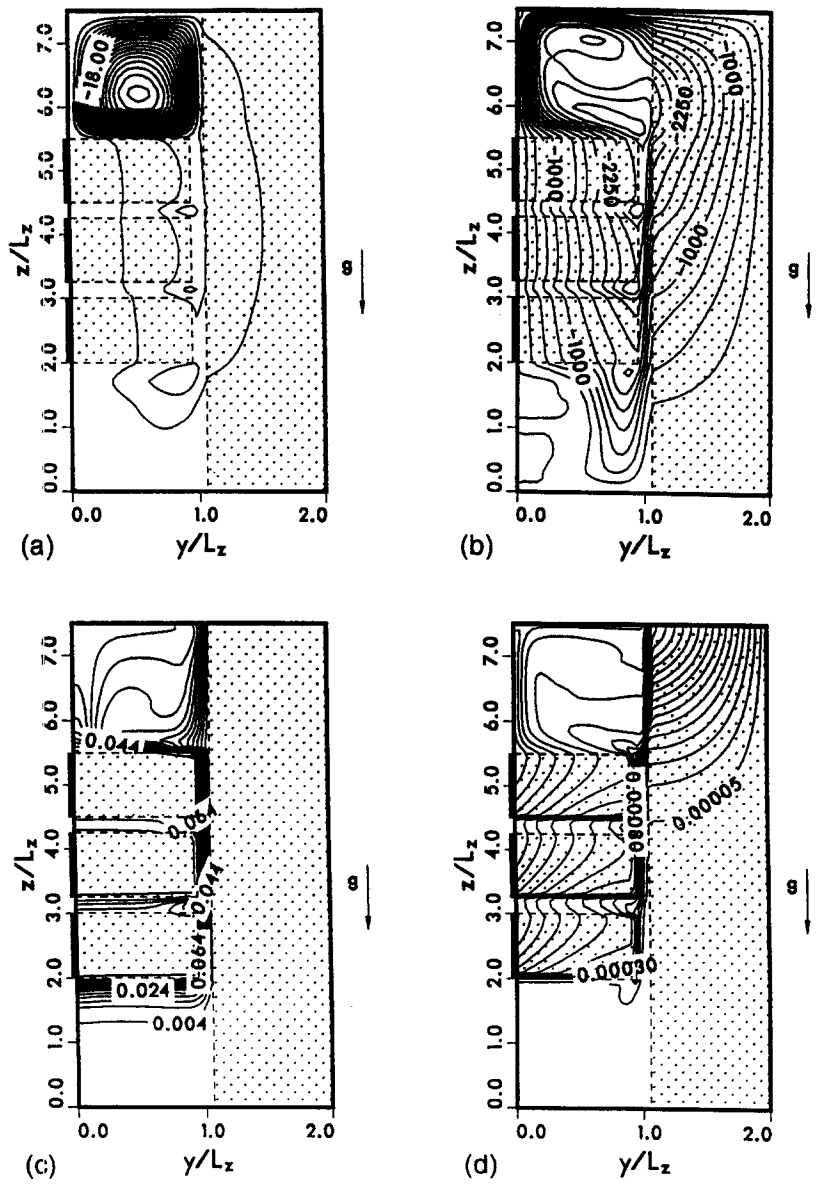

Fig. 6. Dimensionless streamlines (Ψ) at (a) $Ra^*_{L_z} = 10^6$, (b) $Ra^*_{L_z} = 10^{11}$ and isotherms (θ) at (c) $Ra^*_{L_z} = 10^6$, (d) $Ra^*_{L_z} = 10^{11}$ for $Pr = 25$, $A_z = 3.75$ and $Da_b = 6.0 \times 10^{-2}$.

heimer–extended Darcy model providing better overall agreement with the data. Failure of the porous medium model to more accurately predict the experimental results can be attributed to the 2D approximation and the assumption of uniform conditions in the x-direction. Experimentally, preferred flow lanes develop between the heater columns, which result in diminished velocities in the finned regions and an increased thermal resistance. This behavior is most evident in row 3, where the lowest and highest thermal resistances correspond to the Brinkman–extended Darcy model predictions and the experimental data, respectively. However, despite the simplifying assumptions inherent in the 2D porous medium model, it provides a good approximation to the results of a dense parallel plate fin array. This conclusion is supported by visual observations, which revealed flow patterns qualitatively similar to those predicted numerically.

CONCLUSIONS

Relative to unfinned conditions, discrete heat sources with parallel plate fin arrays experienced heat transfer enhancement by as much as 24 and 15 times for ver-

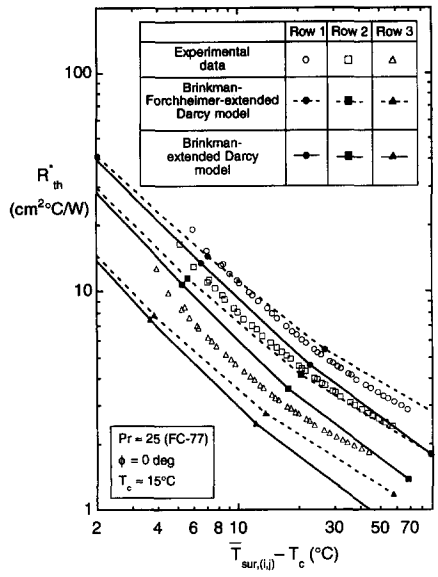

Fig. 7. Comparison between predicted and measured row-averaged thermal resistances.

tical and horizontal cavity orientations, respectively. Maximum heat fluxes were 23.6 W cm^{-2} (vertical cavity, $\Delta T_{max} \approx 70°C$) and 28.2 W cm^{-2} (horizontal cavity, $\Delta T_{max} \approx 65°C$), with corresponding thermal resistances of approximately 2 cm^2°C W^{-1}. The horizontal orientation yielded nearly uniform heat transfer from the discrete heat sources, which is a highly desirable feature when cooling electronic components.

A porous medium model has been used to simulate fluid flow and heat transfer from a dense array of parallel plate fins mounted to one wall of a vertical cavity. Fluid penetration and heat transfer increase within the porous regions as the applied power (modified Rayleigh number) increases. Numerical predictions are in reasonable agreement with experimental results for the vertical orientation, with the Brinkman–Forchheimer–extended Darcy model following the data more closely than the Brinkman–extended Darcy model. Overall, modeling dense parallel plate fin arrays as a porous medium provides a satisfactory approximation.

Acknowledgements—Support of this work by the National Science Foundation under Grant No. CTS-9004213 is gratefully acknowledged. Donation of the parallel plate fin arrays by Technical Materials, Inc., of Lincoln, RI, and the assistance of Mr Joseph P. Mennucci of TMI are also greatly appreciated.

REFERENCES

1. G. P. Peterson and A. Ortega, Thermal control of electronic equipment and devices. In *Advances in Heat Transfer*, Vol. 20 (Edited by J. P. Hartnett and T. F. Irvine Jr.), pp. 181–314 (1990).
2. F. P. Incropera, Convection heat transfer in electronic equipment cooling, *J. Heat Transfer* **110,** 1097–1111 (1988).
3. A. Bar-Cohen, Thermal management of electronic components with dielectric liquids, *Proceedings of the ASME/JSME Thermal Engineering Joint Conference*, Vol. 2 (Edited by J. R. Lloyd and Y. Kurosaki), pp. xv–xxxix (1991).
4. A. D. Kraus and A. Bar-Cohen, *Thermal Analysis and Control of Electronic Equipment*. Hemisphere, New York (1983).
5. Y. H. Hung and C. T. Lu, Optimum-spacing design of vertical PCB arrays in natural convection. In *Transport Phenomena in Thermal Control* (Edited by G.-J. Hwang), pp. 151–161. Hemisphere, New York (1989).
6. W. Elenbaas, Heat dissipation of parallel plates by free convection, *Physica* **9,** 1–28 (1942).
7. K. E. Starner and H. N. McManus, Jr, An experimental investigation of free convection heat transfer from rectangular fin arrays, *J. Heat Transfer* **85,** 273–278 (1963).
8. J. R. Welling and C. B. Wooldridge, Free convection heat transfer coefficients from rectangular vertical fins, *J. Heat Transfer* **87,** 439–444 (1965).
9. J. B. Chaddock, Free convection heat transfer from vertical rectangular fin arrays, *ASHRAE J.* **76,** 53–60 (1970).
10. A. Bar-Cohen, Fin thickness for an optimized natural convection array of rectangular fins, *J. Heat Transfer* **101,** 564–566 (1979).
11. A. Bar-Cohen and W. M. Rohsenow, Thermally optimum spacing of vertical, natural convection cooled, parallel plates, *J. Heat Transfer* **106,** 116–123 (1984).
12. A. Bar-Cohen and M. Jelinek, Optimization of longitudinal finned arrays—London's 25 KW power-tube revisited. In *Compact Heat Exchangers* (Edited by R. K. Shah, A. D. Kraus and D. Metzger), pp. 105–120. Hemisphere, New York (1990).
13. T. Aihara and S. Maruyama, Optimum design of natural cooling heat sinks with vertical rectangular fin arrays. In *Cooling Technology for Electronic Equipment* (Edited by W. Aung), pp. 35–54. Hemisphere, New York (1988).
14. N. K. Anand, S. H. Kim and L. S. Fletcher, The effect of plate spacing on free convection between heated parallel plates, *J. Heat Transfer* **114,** 515–518 (1992).
15. C. Beckermann, R. Viskanta, and S. Ramadhyani, A numerical study of non-Darcian natural convection in a vertical enclosure filled with a porous medium, *Numer. Heat Transfer* **10,** 557–570 (1986).
16. C. Beckermann, R. Viskanta and S. Ramadhyani, Natural convection in vertical enclosures containing simultaneously fluid and porous layers, *J. Fluid Mech.* **186,** 257–284 (1988).
17. V. Srinivasan, K. Vafai, and R. N. Christensen, Analysis of heat transfer and fluid flow through a spirally fluted tube using a porous substrate approach, *J. Heat Transfer* **116,** 543–551 (1994).
18. T. J. Heindel, A numerical and experimental study of three-dimensional natural convection in a discretely heated cavity, Ph.D. Thesis, Purdue University, West Lafayette, IN (1994).
19. S. J. Kline and F. A. McClintock, Describing uncertainties in single-sample experiments, *Mech. Engng* **75,** 3–8 (1953).
20. G. Lauriat and V. Prasad, Non-Darcian effects on natural convection in a vertical porous enclosure, *Int. J. Heat Mass Transfer* **32,** 2135–2148 (1989).
21. C. L. Tien and K. Vafai, Convective and radiative heat transfer in porous media, *Adv. Appl. Mech.* Vol. **27,** 225–281 (1990).
22. J. Bear, *Dynamics of Fluids in Porous Media*. Elsevier, New York (1972).
23. A. Bejan, The method of scale analysis: natural convection in porous media. In *Natural Convection Fun-*

damentals and Applications (Edited by S. Kakaç, W. Aung and R. Viskanta), pp. 549–572. Hemisphere, Washington (1985).
24. G. Lauriat and V. Prasad, Natural convection in a vertical porous cavity: a numerical study for Brinkman–extended Darcy formulation, *J. Heat Transfer* **109,** 688–696 (1987).
25. D. A. Nield and A. Bejan, *Convection in Porous Media.* Springer, New York (1992).
26. S. Ergun, Fluid flow through packed columns, *Chem. Engng Prog.* **48,** 89–94 (1952).
27. G. Neale and W. Nader, Practical significance of Brinkman's extension of Darcy's law: coupled parallel flows within a channel and a bounding porous medium, *Can. J. Chem. Engng* **52,** 475–478 (1974).
28. C. Beckermann, S. Ramadhyani and R. Viskanta, Natural convection flow and heat transfer between a fluid layer and a porous layer inside a rectangular enclosure. In *Natural Convection in Porous Media* (Edited by V. Prasad and N. A. Hussain), ASME HTD-Vol. 56, pp. 1–12 (1986).
29. E. Tsotsas and H. Martin, Thermal conductivity of packed beds: a review, *Chem. Engng Proc.* **22,** 19–37 (1987).
30. E. Hahne, Y. W. Song and U. Gross, Measurements of thermal conductivity in porous media, *ASI Proceedings 1990—Convection Heat and Mass Transfer in Porous Media,* Izmir, Turkey, pp. 523–539 (1990).
31. S. V. Patankar, *Numerical Heat Transfer and Fluid Flow.* Hemisphere, New York (1980).
32. B. R. Hutchinson and G. D. Raithby, A multigrid method based on the additive correction strategy, *Numer. Heat Transfer* **9,** 511–537 (1986).
33. B. R. Hutchinson, P. F. Galpin and G. D. Raithby, Application of additive correction multigrid to the coupled fluid flow equations, *Numer. Heat Transfer* **13,** 133–147 (1988).
34. M. S. Polentini, S. Ramadhyani and F. P. Incropera, Single-phase thermosyphon cooling of an array of discrete heat sources in a rectangular cavity, *Int. J. Heat Mass Transfer* **36,** 3983–3996 (1993).

APPENDIX: FIN DESIGN AND FABRICATION

The parallel plate fin arrays employed in this study were designed for maximum power dissipation. The plate spacing required to maximize heat transfer from adjacent parallel plates would provide for boundary layer merger at the trailing edge of the heat transfer surface. However, in an array of parallel plate fins, that fin spacing may not correspond to the maximum total power dissipation. As more fins are added to the array, the heat transfer surface area increases. Eventually, if the fins are too closely spaced, heat transfer from each fin is substantially reduced and total power dissipation from the array may decrease, even though more surface area is added. Therefore, an optimum geometry exists to maximize total power dissipation from a fin array.

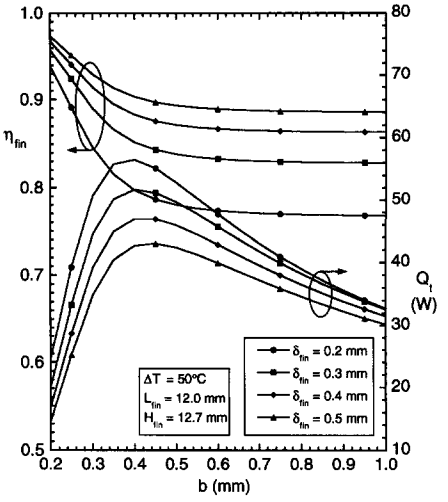

Fig. A1. Fin efficiency and total power dissipation rate for a parallel plate fin array with a heated base area of 12.7 mm × 12.7 mm.

To determine this optimum, the fin length was fixed ($L_{fin} = 12$ mm), as were the heater base dimensions ($L_x = L_z = H_{fin} = 12.7$ mm). The fin material (copper) and heat transfer fluid (FC-77) were also fixed, and a maximum allowable temperature difference of 50°C was prescribed between the fin base and the reference fluid. If the fin length is much larger than the fin spacing ($L_{fin}/b \gg 1$), edge effects at the fin base and tip may be neglected and flow between the fins can be approximated as two-dimensional. Assuming that the fin efficiency is high and the fins are approximately isothermal, equation (1) can then be used to estimate the average heat transfer coefficient for the fin face ($\bar{h} = \overline{Nu}_b k_f/b$). The power dissipation rate per fin can then be calculated as $Q_{fin} = \eta_{fin}\bar{h}A_{fin}(T_{sur} - T_r)$, where A_{fin} is the total fin surface area and, assuming an adiabatic tip, the fin efficiency may be approximated as $\eta_{fin} = \tanh(mL_{fin})/(mL_{fin})$. The total power dissipation from the fin array is then $Q_t = N_{fin}Q_{fin}$, where the total number of fins per heat source, N_{fin}, depends on the selection of δ_{fin} and b. This expression neglects heat transfer from the base area between fins, as well as from all fin edges.

Calculations based on the foregoing model are presented in Fig. A1, where the fin efficiency and total power dissipation are plotted as a function of fin spacing for different fin thicknesses. For $0.2 \leqslant \delta_{fin} \leqslant 0.5$ mm, maximum power dissipation corresponds to an optimum fin spacing of $0.35 \lesssim b \lesssim 0.45$ mm. A similar procedure was used to design the finned cold

Table A1. Fin dimensions associated with the parallel plate fin arrays

	Heater array	Cold plate array
L_z	12.7 mm	95.3 mm
L_x	12.7 mm	57.2 mm
H_{fin}	12.7 mm	91.4 mm
L_{fin}	12.0 mm	12.0 mm
δ_{fin}	0.20 mm	0.20 mm
b	0.51 mm	0.51 mm
N_{fin}	18	72
Increase in heat transfer surface area	~35 times	~30 times
k_{fin}	400 W m^{-1} K^{-1}	400 W m^{-1} K^{-1}
k_f	0.0631 W m^{-1} K^{-1}	0.0631 W m^{-1} K^{-1}

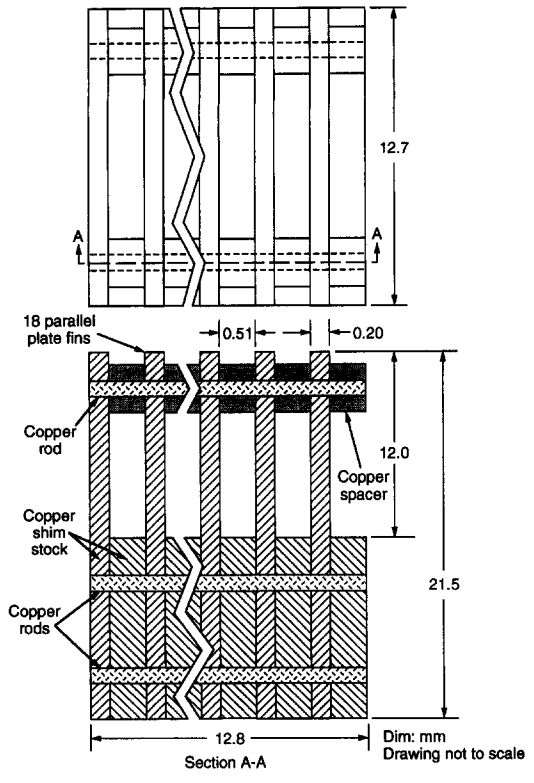

Fig. A2. Schematic representation of a single finned heat source.

plate attachment [18], and for $0.2 \leqslant \delta_{fin} \leqslant 0.5$ mm, optimization revealed that all of the energy from the heaters could be absorbed if the cold plate fin spacings were in the range $0.55 < b < 0.75$ mm.

To facilitate manufacturability and reduce costs, the same fin thickness and spacing were prescribed for the heater and cold plate fin arrays. A fin thickness and spacing of $\delta_{fin} = 0.20$ mm and $b = 0.51$ mm provided a good compromise between maximum power dissipation/absorption rates and efficiencies of the heater and cold plate fins. Complete fin dimensions for each heat source and the cold plate are summarized in Table A1. To allow for easy assembly, the cold plate fin height ($H_{fin} = 91.4$ mm) is slightly smaller than the cavity height ($H = 95.3$ mm), and the cold plate fins covered 53.3 mm of the 57.7 mm cavity depth.

An assembly schematic of the plate fin array for a single heater is shown in Fig. A2. The fin array was fabricated by Technical Materials, Inc. (TMI) of Lincoln, RI, using a proprietary copper bonding process called Direct Bond Copper (DBC). In this process, the fin and base sections were stamped from copper shim stock of the prescribed thicknesses, with included holes used for assembly. An array was assembled by positioning the fin and base shim stock, in an alternating fashion, on very small diameter copper rods inserted through the holes left by the stamping process. To maintain dimensional integrity of the fin spacing, as well as fin rigidity and strength, additional rods were located at the top of the fin arrays (two in each heat source and four in the cold plate). The spacing between fins was preserved by placing small copper spacers (washers), with the same thickness as the base shim stock, on the rods located in the fin tips. Each fin assembly was then compressed in the rod direction, and the direct bond process was effected by placing it in an oven programmed to follow a prescribed temperature history.